PERGAMON

International Journal of Solids and Structures 37 (2000) 4987–5008

INTERNATIONAL JOURNAL OF SOLIDS and STRUCTURES

www.elsevier.com/locate/ijsolstr

An effective boundary element algorithm for 2D and 3D elastoplastic problems

Xiao-Wei Gao*, Trevor G. Davies

Department of Civil Engineering, Glasgow University, Glasgow, G12 8LT, UK

Received 26 February 1999; in revised form 25 May 1999

Abstract

Novel methods are described for removing the strong singularities arising in the domain integrals of elastoplasticity, and for solving the non-linear equation set. The former employs a new transformation from domain integrals to (cell) boundary integrals. The number of system equations is minimised by using the plastic multiplier as the primary unknown and an incremental variable stiffness iterative algorithm is developed for solving these equations. Excellent convergence is achieved and some numerical examples demonstrate the algorithm's effectiveness. © 2000 Elsevier Science Ltd. All rights reserved.

Keywords: Boundary element method; Elastoplastic problem; Singular domain integral; Variable stiffness iteration; Plastic multiplier

1. Introduction

The earliest work on non-linear boundary element method (BEM) was done by Swedlow and Cruse (1971), Riccardella (1973) and Mendelson and Albers (1975). Some errors in the earlier formulations were corrected by Mukherjee (1977), Bui (1978) and Telles and Brebbia (1979). However, some inherent difficulties, such as the strongly singular domain integrals and the stability of the system equations, have stymied development of this method.

One of the crucial tasks in the non-linear BEM is to remove (or regularise) the strong singularities arising in the domain integrals. The existing methodologies may be categorised as follows:

1. Interpolation using nodal displacements (differentiating the shape functions) (Banerjee et al., 1979; Gao and Lu, 1992; Wearing and Dimagiba, 1998).

* Corresponding author. fax: +44-141-330-4557.
E-mail address: Gao@civil.gla.ac.uk (X.W. Gao).

0020-7683/00/$ - see front matter © 2000 Elsevier Science Ltd. All rights reserved.
PII: S0020-7683(99)00188-2

2. Analytical and semi-analytical techniques (Riccardella, 1973; Mendelson and Albers, 1975; Telles and Brebbia, 1979; Zheng and Gao, 1986; Zheng et al., 1989; Chandra and Saigal, 1991).
3. Exclusion of a small sphere using higher order volume cells (Banerjee and Davies, 1984; Banerjee and Raveendra, 1986).
4. Transformation of domain integrals to surface integrals (Huang and Du, 1988; Zhang et al., 1992; Dallner and Kuhn, 1993; Chandra and Mukherjee, 1996; Chen et al., 1996; Dong and Antes, 1998).
5. Regularisation of singular integrals (Guiggiani and Gigante, 1990; Guiggiani et al., 1992; Huber et al., 1996; Cisilino et al., 1998; Poon et al., 1998a; Burghardt and Van, 1998).
6. Indirect approaches (Telles and Brebbia, 1979; Brebbia et al., 1984; Lee and Fenner, 1986; Chen and Ji, 1987; Henry and Banerjee, 1988; Banerjee et al., 1989).

In category 1, the internal stresses are calculated using nodal displacements by differentiating the shape functions using methods employed in FEM. Due to the properties of the shape functions and their derivatives, this local procedure is prone to significant deviations especially in the case of coarse meshes and low order shape functions. Category 2 is only feasible with 'constant' or 'linear' cells, in which the singularities of the initial stress (strain) kernels can be eliminated analytically or semi-analytically. In category 3, the strongly singular domain integrals become bounded, if a small sphere around the singular point is excluded. Although this method can deal with higher order cells, with the help of the volume sub-division technique which is originally proposed by Lachat (1975) and coded by Mustoe (1984), it may give inaccurate results for cases in which the cells around the singular point are greatly different in shape or size.

In category 4, the singularity is first isolated by subtracting singular function from the original singular integral. The subtracted integral becomes weakly singular, which can then be integrated using standard Gauss quadrature. The singular function is transformed, via Gauss theorem, into a regular surface integral over the boundary of the body or plastic region. A rather different transformation was employed by Dallner and Kuhn (1993) in their initial strain algorithm. In their work, the transformed surface integral is mapped over the boundary of the elements surrounding the source point rather than over the body's surface.

Another approach (category 5) for direct evaluation of principal value integrals was suggested by Guiggiani and Gigante (1990), based on the regularisation of the singular integral by subtracting the truncated Taylor series from the integrand. Although, in principle, this method can also be used for evaluation of singular surface integrals (Guiggiani et al., 1992), it is feasible only for smooth boundary points. All functions must be expressed in a local spherical co-ordinate system. Then all integrands, including kernels, spatial derivatives, Jacobians and shape functions are expanded in Taylor series form, in terms of the local co-ordinates. As a consequence, the calculations are tedious and complicated, and difficult to implement in a computer code. Another type of regularisation for directly calculating the boundary stresses is developed by Poon et al. (1998a). A simple equation was obtained by the use of three global modes of deformation: rigid-body displacement, linear displacement, and a fully constrained plastic solution. While their approach is relatively straightforward, computation would be enormous, since the system equations now involve stresses, displacements and displacement gradients.

In the last category 6, the singularities can be circumvented by employing indirect approaches, based on the application of known reference solutions. The drawback of this approach is that it requires discretization of the cells through the entire region, which negates to a certain extent the advantage of BEM (namely, that only the yield zone needs to be discretised into cells). To avoid this discretization, multi-region BEM technique was employed (Banerjee et al., 1989) or a second boundary was defined (Lee and Fenner, 1986).

Another important task in non-linear BEM is the solution strategy for solving the system equations.

Several algorithms using domain discretization methods have been developed. More often than not the algorithms are 'explicit' as described in detail by Telles (1983) and Banerjee (1994). These solution algorithms can be roughly divided into two groups, i.e., the initial strain approach (Riccardella, 1973; Mendelson and Albers, 1975; Kumar and Mukherjee, 1977; Telles and Brebbia, 1979, 1980; Lee and Fenner, 1986; Kane, 1994; Cisilino et al., 1998) and the initial stress approach (Banerjee et al., 1979; Banerjee and Davies, 1979; Raveendra, 1984; Zheng and Gao, 1986; Henry, 1987; Chopra and Dargush, 1994).

More recently, several researchers have investigated implicit solution schemes, on account of their unconditional stability (Telles and Carrer, 1991; Bonnet and Mukherjee, 1996; Poon et al., 1998b; Burghardt and Van, 1998; Gao, 1999). Among these works, Bonnet and Mukherjee (1996) first applied the *consistent tangent operator* method to boundary element method. This method, which was first proposed by Simo and Taylor (1985) in the finite element method context, exploits the quadratic rate of convergence which can be achieved by utilising consistent elastoplastic constitutive relations in the Newton–Raphson iterative process. Although this iterative method is relatively easy to code, it requires considerable computer memory. This is because the system equations are formulated in terms of strain increments, which have six degrees of freedom at each node for 3D problems. Even if the block decomposition technique is employed, as described by Bonnet and Mukherjee (1996), the computer memory requirement is substantial.

A different type of solution strategy (*incremental variable stiffness*) has been successfully demonstrated by Banerjee and his co-workers (Raveendra, 1984; Banerjee et al., 1989; Banerjee, 1994). In this scheme, the internal variables are eliminated, by expressing them in terms of boundary variables, and consequently no iteration is needed, if small increments are used. Chopra and Dargush (1994) described a Newton–Raphson solution algorithm for solving the non-linear system equations, in which both the boundary unknowns and plastic multipliers were used as primary unknowns of the system equations.

In this paper, novel methods are presented for removing the strong singularities arising in the domain integrals in evaluating interior stresses and for solving the non-linear system of equations. New identities for the initial stress and strain kernels are derived, and a novel technique is used to transform the domain integrals into (cell) boundary integrals, in order to remove the strong singularities. The results are suitable for both 2D and 3D problems, linear and higher order cells, and both initial stress and strain approaches. To solve the system equations, a novel incremental variable stiffness iterative algorithm is proposed based on the Newton–Raphson iterative scheme. In this algorithm, the plastic multipliers (only) are used as the primary unknowns, with the result that the number of degrees of freedom is equal to the number of yielded nodes in the current increment. Consequently, both computational time and computer memory are substantially reduced. Rapid convergence is achieved by using the Newton–Raphson iterative procedure as demonstrated by some numerical examples.

2. BEM formulation of elasto-plasticity

For a region Ω bounded by a boundary Γ, the direct formulation of the boundary integral equations for elasto-plasticity can be expressed in the incremental form (Swedlow and Cruse, 1971; Telles and Brebbia, 1979; Banerjee and Raveendra, 1986):

$$c_{ij}(P)\dot{u}_j(P) + \int_\Gamma T_{ij}(P, Q)\dot{u}_j(Q)\,\mathrm{d}\Gamma(Q) = \int_\Gamma U_{ij}(P, Q)\dot{t}_j(Q)\,\mathrm{d}\Gamma(Q) + \int_\Omega E_{ijk}(P, q)\dot{\sigma}^p_{jk}(q)\,\mathrm{d}\Omega(q) \tag{1}$$

where $T_{ij}(P, Q)$ and $U_{ij}(P, Q)$ are the Kelvin fundamental solutions for tractions (t) and displacements (u) at a point Q in the jth direction due to a unit load at point P and $E_{ijk}(P, q)$ is the corresponding

strain kernel:

$$E_{ijk} = \frac{-1}{8\pi(\beta-1)(1-\nu)Gr^{\beta-1}}\{(1-2\nu)(r_{,k}\delta_{ij} + r_{,j}\delta_{ik}) - r_{,i}\delta_{jk} + \beta r_{,i}r_{,j}r_{,k}\} \tag{2}$$

$$r_{,i} = \frac{r_i}{r}, \quad r_i = x_i(Q) - x_i(p) \tag{3}$$

where, $\beta = 3$ in three dimensions and $\beta = 2$ in plane-strain; r is the distance between the source point p and the field point Q.

In Eq. (1), $c_{ij}(P) = 1/2\delta_{ij}$ for smooth boundary points. The strongly singular terms arising from the integration of the traction kernel are determined indirectly using the rigid body (translation) condition. Eq. (1) is also used to calculate the displacements at an interior point p by replacing $c_{ij}(P) = 1/2\delta_{ij}$ with $c_{ij}(p) = \delta_{ij}$.

The initial stress increment $\dot{\sigma}^p_{ij}$ can be defined in terms of the plastic strain increment as:

$$\dot{\sigma}^p_{ij} = D^e_{ijkl}\dot{\varepsilon}^p_{kl} \tag{4}$$

where D^e_{ijkl} is the elastic constitutive tensor. Interior strain increments $\dot{\varepsilon}_{kl}$ can be found by differentiating Eq. (1) with respect to the source point p. Then, using the following relationship (e.g., Banerjee and Davies, 1984):

$$\dot{\sigma}_{ij} = D^e_{ijkl}(\dot{\varepsilon}_{kl} - \dot{\varepsilon}^p_{kl}) = D^e_{ijkl}\frac{\partial \dot{u}_k}{\partial x_l} - \dot{\sigma}^p_{ij} \tag{5}$$

the stress increments $\dot{\sigma}_{ij}$ at an interior point p can be found as

$$\begin{aligned}\dot{\sigma}_{ij}(p) = &\int_\Gamma U_{ijk}(p,Q)\dot{t}_k(Q)\,\mathrm{d}\Gamma(Q) - \int_\Gamma T_{ijk}(p,Q)\dot{u}_k(Q)\,\mathrm{d}\Gamma(Q)\\ &+ \int_\Omega E_{ijkl}(p,q)\dot{\sigma}^p_{kl}(q)\,\mathrm{d}\Omega(q) + F^\sigma_{ij}(\dot{\sigma}^p_{kl})\end{aligned} \tag{6}$$

where $F^\sigma_{ij}(\dot{\sigma}^p_{kl})$ are the free terms (e.g., Telles, 1983; Banerjee, 1994), and

$$E_{ijkl} = D^e_{ijmn}\frac{\partial E_{mkl}}{\partial x_n(p)} = \frac{\Psi_{ijkl}}{r^\beta} \tag{7}$$

in which

$$\begin{aligned}\Psi_{ijkl} = \frac{1}{4\pi(\beta-1)(1-\nu)}&[(1-2\nu)(\delta_{ik}\delta_{lj} + \delta_{jk}\delta_{li} - \delta_{ij}\delta_{kl} + \beta\delta_{ij}r_{,k}r_{,l}) + \beta\nu(\delta_{li}r_{,j}r_{,k} + \delta_{jk}r_{,l}r_{,i}\\ &+ \delta_{ik}r_{,l}r_{,j} + \delta_{jl}r_{,i}r_{,k}) + \beta\delta_{kl}r_{,i}r_{,j} - \beta(\beta+2)r_{,i}r_{,j}r_{,k}r_{,l}]\end{aligned} \tag{8}$$

In the initial strain approach, the terms E_{ijkl}, $\dot{\sigma}^p_{kl}$ and the free term $F^\sigma_{ij}(\dot{\sigma}^p_{kl})$ should be replaced, respectively, with Σ_{ijkl}, $\dot{\varepsilon}^p_{kl}$ and $F^\varepsilon_{ij}(\dot{\varepsilon}^p_{kl})$ (Telles, 1983; Banerjee, 1994).

The integrals in Eqs. (1) and (6) should be interpreted in the Cauchy principal value sense. After use of the cell sub-division technique (Banerjee and Davies, 1984; Mustoe, 1984), the weakly singular domain integral in Eq. (1) involving the kernel E_{ijk} is bounded, while the strongly singular domain integral in Eq. (6) involving the kernel E_{ijkl} is still singular, with order $1/r$. Special integration techniques

must therefore be adopted in order to make the integral bounded. One direct method is to exclude a small sphere around the singular point p (Banerjee and Davies, 1984). This technique gives useful results only for some special cases. A new efficient method for removing the strong singularity is presented in the following section.

3. Accurate evaluations of strongly singular domain integrals

The most popular method for treating strongly singular integrals consists of two steps, namely, isolation and transformation of the singularity (e.g., Krishnasamy et al., 1992). In this paper, the singularity is first isolated by subtracting a singular function from the original kernel so that the subtracted term becomes a weakly singular one, which can then be evaluated by standard numerical integration procedures. The isolated strongly singular integral is then evaluated by integral transformation, based on the novel identities established below.

3.1. Identities for integrations of strongly singular kernels

To evaluate the domain integrals, the region is usually discretized into cells. For the cells including the source point p, the domain integrals in Eq. (6) can be written as:

$$\int_{\Omega} E_{ijkl}(p,q)\dot{\sigma}^{p}_{kl}(q)\,\mathrm{d}\Omega(q) = \int_{\Omega} E_{ijkl}(p,q)\left[\dot{\sigma}^{p}_{kl}(q) - \dot{\sigma}^{p}_{kl}(p)\right]\mathrm{d}\Omega(q) + \dot{\sigma}^{p}_{kl}(p)\left[\int_{\Omega} E_{ijkl}(p,q)\,\mathrm{d}\Omega(q)\right] \tag{9}$$

Now the first integral on the right-hand side of Eq. (9) is weakly singular and can be evaluated by the cell sub-division technique (Mustoe, 1984), while the strong singularity is shifted to the second integral of the right-hand side. To remove this singularity, firstly we examine the integration of the kernel E_{ijkl} over a sphere centred at p with a radius R (Fig. 1).

For such a sphere, from Eq. (7) we have

$$\int_{\Omega_R} E_{ijkl}\,\mathrm{d}\Omega = \int_0^R \frac{1}{r^{\beta}}\left(\int_{S_r} \Psi_{ijkl}\,\mathrm{d}S\right)\mathrm{d}r \tag{10}$$

where S_r is the spherical surface (or circle) with radius r for 3D (or 2D) problems. Using a spherical (or polar) coordinate system centered at p, we can obtain (Gao, 1999):

$$\int_{S_r} \delta_{ij}\,\mathrm{d}S = 2\pi(\beta-1)\delta_{ij}r^{\beta-1}$$

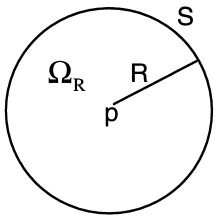

Fig. 1. A sphere with radius R.

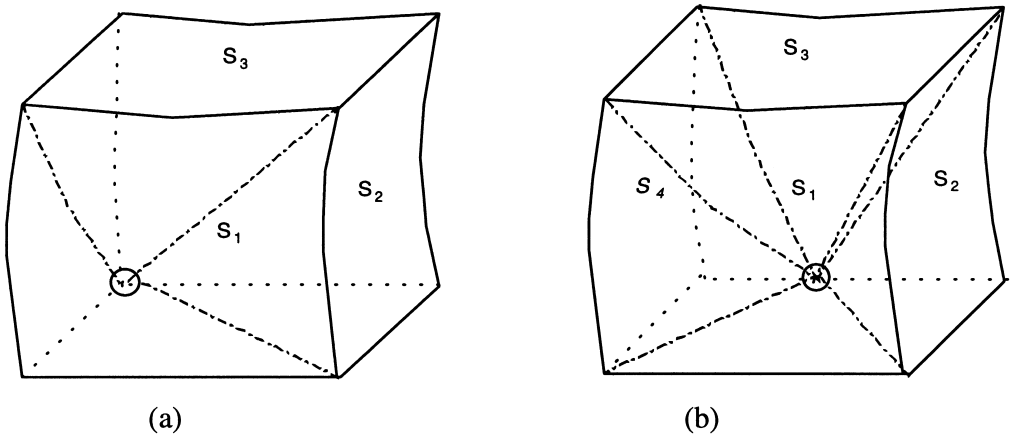

Fig. 2. Cell sub-division: (a) p at the corner; (b) p at mid-side.

$$\int_{S_r} r_{,i} r_{,j}\, \mathrm{d}S = \frac{2\pi(\beta-1)}{\beta}\delta_{ij} r^{\beta-1}$$

$$\int_{S_r} r_{,i} r_{,j} r_{,k} r_{,l}\, \mathrm{d}S = \frac{2\pi(\beta-1)}{\beta(\beta+2)}\left(\delta_{ij}\delta_{kl} + \delta_{ik}\delta_{jl} + \delta_{il}\delta_{jk}\right) r^{\beta-1} \tag{11}$$

Substituting Eq. (8) into (10) and using Eq. (11) leads to the identity:

$$\int_{S_r} \Psi_{ijkl}\, \mathrm{d}S = 0 \tag{12}$$

So from Eq. (10), we obtain

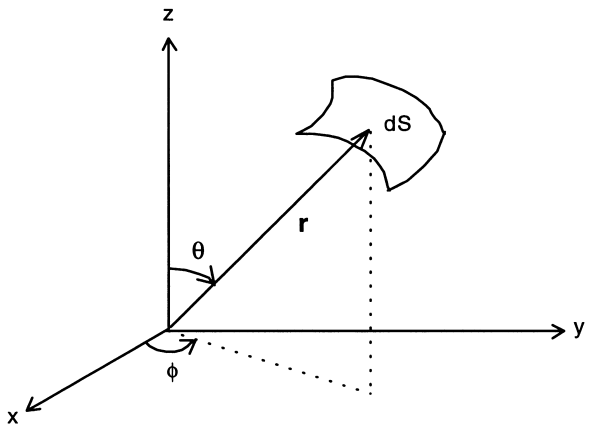

Fig. 3. Local spherical co-ordinate system.

$$\int_{\Omega_R} E_{ijkl}\,\mathrm{d}\Omega = 0 \tag{13}$$

In a similar way, for the initial strain approach, we can obtain

$$\int_{\Omega_R} \Sigma_{ijkl}\,\mathrm{d}\Omega = 0 \tag{14}$$

Identities (12)–(14) are valid for a sphere (or circle) of arbitrary radius and provide the basis of accurately evaluating the strongly singular domain integrals.

3.2. Transformation of the strongly singular domain integrals into cell boundary integrals

In this section, only 3D problems are considered since the application of the results to 2D problems is straightforward. A cell, including the source point p, is sub-divided into three tetrahedra (when p is located at a corner node) or four tetrahedra (when p is located at a mid-side node). These tetrahedra are defined by a vertex at point p and those surfaces of the cell not including p (Fig. 2). For each tetrahedron, we define a spherical co-ordinate system with origin at p (Fig. 3):

For such a co-ordinate system, we have:

$$\mathrm{d}\Omega = \mathrm{d}r\,\mathrm{d}S \tag{15}$$

where the differential element on the spherical surface ($\mathrm{d}S$) is:

$$\mathrm{d}S = r^2 \sin\theta\,\mathrm{d}\theta\,\mathrm{d}\phi \tag{16}$$

Let us consider the integral of E_{ijkl} over a sub-cell Ω_c^s. Because the integration is carried out in the Cauchy principal value sense, we can cut off a small sphere with radius ε around the singular point p (Fig. 4).

Thus from Eqs. (7) and (8), we can see that if Eqs. (15) and (16) are substituted into the last integral on the right-hand side of Eq. (9), the domain integration over the sub-cell Ω_c^s can be separated into a radial part and a spherical surface part, i.e.,

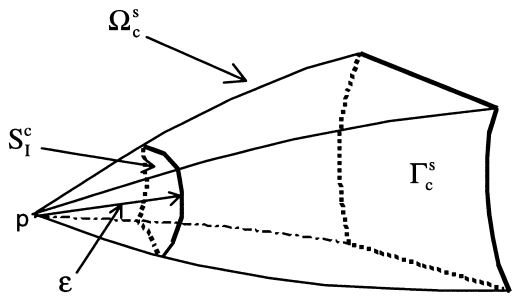

Fig. 4. Small exclusion cut off from a sub-cell Ω_c^s.

$$\int_{\Omega_c^s} E_{ijkl}\,\mathrm{d}\Omega = \int \Psi_{ijkl}\left(\lim_{\varepsilon\to 0}\int_{\varepsilon}^{r(\Gamma_c^s)} \frac{1}{r}\,\mathrm{d}r\right)\mathrm{d}S_{\mathrm{I}}$$

$$= \int_{\Gamma_c^s} \Psi_{ijkl}\ln r\left(\Gamma_c^s\right)\mathrm{d}S_{\mathrm{I}} - \lim_{\varepsilon\to 0}\ln\varepsilon\int_{S_{\mathrm{I}}^c}\Psi_{ijkl}\,\mathrm{d}S_{\mathrm{I}} \tag{17}$$

where $\mathrm{d}S_{\mathrm{I}}$ is a differential element on the spherical surface with unit radius, i.e.,

$$\mathrm{d}S_{\mathrm{I}} = \frac{\mathrm{d}S}{r^2} = \sin\theta\,\mathrm{d}\theta\,\mathrm{d}\phi \tag{18}$$

Summing for all cells, the result $\sum_c S_{\mathrm{I}}^c$ forms a closed spherical surface, so according to identity (12) the last integral in Eq. (17) is zero. Furthermore, with the help of Fig. 5, we have:

$$\mathrm{d}S = \mathrm{d}\Gamma\cos\beta = \mathrm{d}\Gamma\frac{r_i n_i}{r} \tag{19}$$

where β is the angle between the normal of the differential element of the spherical surface $\mathrm{d}S$ directed along the r direction and the cell boundary surface $\mathrm{d}\Gamma$ with normal n.

Substituting Eq. (19) into (18), it follows that:

$$\mathrm{d}S_{\mathrm{I}} = \frac{r_i n_i}{r^3}\,\mathrm{d}\Gamma \tag{20}$$

Eventually, substituting the above equation into the first integral on the right-hand side of Eq. (17) and using Eq. (7), we obtain:

$$\int_{\Omega_c^s} E_{ijkl}\,\mathrm{d}\Omega = \int_{\Gamma_c^s} E_{ijkl} r_m n_m \ln r\,\mathrm{d}\Gamma \tag{21}$$

Similarly, for the initial strain approach, we can obtain:

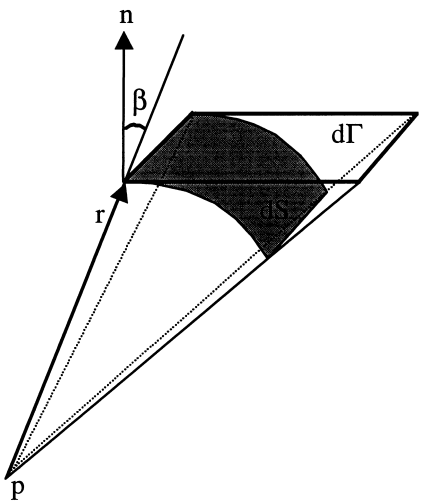

Fig. 5. Relation between spherical surface ($\mathrm{d}S$) and cell boundary ($\mathrm{d}\Gamma$).

$$\int_{\Omega_c^s} \Sigma_{ijkl}\,\mathrm{d}\Omega = \int_{\Gamma_c^s} \Sigma_{ijkl} r_m n_m \ln r\,\mathrm{d}\Gamma \tag{22}$$

Now the domain integrals have been transformed into non-singular cell boundary integrals. They can be calculated using standard Gaussian quadrature formulae. For 2D problems, we can derive exactly the same results, as Eqs. (21) and (22), with the understanding that the boundary integrals are carried out over line elements.

Eqs. (21) and (22) are very easy to use. The kernels of the transformed boundary integrals are simply formed by multiplying the original kernels, E_{ijkl} and Σ_{ijkl}, by the terms, $r_m\ n_m\ \ln r$. The boundary integrals need to be carried out only over the outer surfaces of the volume cells around the source point p. Moreover, they have the same forms for 2D and 3D problems, so simplifying the task of developing unified code.

3.3. Numerical implementation formulation of the strongly singular domain integrals

We assume that the expected yield region is divided into N_c interior cells, each of which forms a piecewise continuous approximation to the yield region. Over each cell, the positional co-ordinates and initial stresses are interpolated using quadratic shape functions. Thus, the strongly singular domain integral in Eq. (6) can be expressed as:

$$\int_{\Omega} E_{ijkl}(p, q)\dot{\sigma}_{kl}^{p}(q)\,\mathrm{d}\Omega(q) = \sum_{c=1}^{N_c}\sum_{\alpha=1}^{N_n} E_{ijkl}^{c\alpha}\dot{\sigma}_{kl}^{p\alpha} \tag{23}$$

where N_n is the number of cell's nodes (20 for 3D and 8 for 2D), and,

$$E_{ijkl}^{c\alpha} = \int_{\Omega_c} E_{ijkl}(p, q)N_\alpha(q)\,\mathrm{d}\Omega(q) \tag{24}$$

in which, Ω_c is the domain of the cell c, $\dot{\sigma}_{ij}^{p\alpha}$ is the ijth component of the initial stress at node α, and N_α are the shape functions (Banerjee, 1994; Gao, 1999).

For cells not including the source point p, Eq. (24) can be calculated in the usual way (for adjacent cells having greatly differing sizes, an adaptive integration algorithm is needed (Gao and Davies, 1999b)). For the cells which include the source point p, the cell Ω_c is sub-divided into a number of sub-cells (Fig. 2), i.e., $\Omega_c = \sum_s^{N_c^s} \Omega_c^s$ with N_c^s being the number of the sub-cells. Using Eqs. (9) and (21) we have:

$$E_{ijkl}^{c\alpha} = \sum_{s=1}^{N_c^s}\int_{\Omega_c^s} E_{ijkl}(p, q)\left\{N_\alpha(q) - \delta_{\alpha p}\right\}\mathrm{d}\Omega(q) + \delta_{\alpha p}\sum_{s=1}^{N_c^s}\int_{\Gamma_c^s} E_{ijkl}(p, Q)r_m n_m \ln r\,\mathrm{d}\Gamma(Q) \tag{25}$$

where

$$\delta_{\alpha p} = \begin{cases} 1 & \text{when } \alpha = p \\ 0 & \text{when } \alpha \neq p \end{cases} \tag{26}$$

The last integral on the right-hand side of Eq. (25) can be performed by the usual boundary integration scheme. However, in the evaluation of the first domain integral, the intrinsic co-ordinate transformation from the original system to a new system established in a sub-cell is necessary (Mustoe, 1984; Gao, 1999).

4. Incremental variable stiffness iterative algorithm

In the numerical implementation, the boundary of the body under consideration is discretized into boundary elements and the expected yield region is discretized into cells. Evaluation of the boundary integrals in Eqs. (1) and (6) can be found in various references (e.g., Swedlow and Cruse, 1971; Telles and Brebbia, 1979; Banerjee and Raveendra, 1986; Mukherjee, 1982; Gao and Davies, 1999a). The weakly singular domain integral in Eq. (1) is performed using the cell sub-division technique (e.g., Mustoe, 1984; Dallner and Kuhn, 1993). The strongly singular domain integrals in Eq. (6) for calculating the interior stresses are evaluated using the method described in the previous section. Stress fields at boundary element nodes are computed using the boundary stress-recovery method (Swedlow and Cruse, 1971; Telles and Brebbia, 1979; Kane, 1994). Finally, from Eqs.(1) and (6) and using the boundary stress-recovery method, we obtain:

$$[H]\{\dot{u}\} = [G]\{\dot{t}\} + \left[E^b\right]\{\dot{\sigma}^p\} \tag{27}$$

$$\{\dot{\sigma}\} = [H^\sigma]\{\dot{u}\} + [G^\sigma]\{\dot{t}\} + [E^\sigma]\{\dot{\sigma}^p\} \tag{28}$$

where $\{\dot{u}\}$ and $\{\dot{t}\}$ are boundary displacement and traction vectors, respectively, and $\{\dot{\sigma}^p\}$ is initial stress vector, consisting of initial stresses at both boundary nodes and interior nodes. After applying the boundary conditions to Eq. (27), transferring all the boundary unknowns to the left-hand side and transferring the known matrix products to the right-hand side, we obtain:

$$\left[A^b\right]\left\{\dot{X}\right\} = \left\{\dot{Y}^b\right\} + \left[E^b\right]\{\dot{\sigma}^p\} \tag{29}$$

where $\{\dot{X}\}$ are the boundary unknowns.

Similarly, after applying the boundary conditions, Eq. (28) yields:

$$\{\dot{\sigma}\} = [A^\sigma]\left\{\dot{X}\right\} + \left\{\dot{Y}^\sigma\right\} + [E^\sigma]\{\dot{\sigma}^p\} \tag{30}$$

where $\{\dot{\sigma}\}$ is a global stress vector, consisting of stresses at both boundary nodes and interior nodes.

To solve Eqs. (29) and (30), expressions for evaluating the initial stress increments must be obtained. In this paper, a strain-space plastic formulation is adopted.

4.1. Rate-independent elastoplastic equations

In the classical (flow) theory of plasticity, the general elastoplastic constitutive relations are based on Drucker's postulate (e.g., Owen and Hinton, 1980; Crisfield, 1997). However, Drucker's postulate is only suitable for stable materials under stress control with perfect plasticity as a limiting case (Naghdi and Trapp, 1975; Gao and Zheng, 1990). In this paper, the elastoplastic constitutive relationships based on Il'iushin's postulate (Il'iushin, 1961) are adopted, which is suitable for both stable and unstable behaviour. For simplicity, the following yield function is considered (for more general cases, see Gao, 1999):

$$F\left(\sigma_{ij}, \varepsilon^p_{kl}, \bar{\varepsilon}^p\right) = f\left(\sigma_{ij}, \varepsilon^p_{kl}, \bar{\varepsilon}^p\right) - k(\bar{\varepsilon}^p) = 0 \tag{31}$$

where $\bar{\varepsilon}^p$ is the equivalent plastic strain. Its increment is given by:

$$\dot{\bar{\varepsilon}}^p = \sqrt{\frac{2}{3}\dot{\varepsilon}^p_{ij}\dot{\varepsilon}^p_{ij}} \tag{32}$$

The Il'iushin postulate states that the work done in a closed strain cycle is non-negative and yields the following results (e.g., Chen and Han, 1988; Gao and Zhong, 1992):

$$\dot{\sigma}_{ij}^{p} = \dot{\lambda} D_{ijkl}^{e} \frac{\partial f}{\partial \sigma_{kl}} \tag{33}$$

where $\dot{\lambda}$ is the plastic multiplier, which is given by (e.g., Gao, 1999):

$$\dot{\lambda} = \frac{1}{\psi} \frac{\partial f}{\partial \sigma_{ij}} D_{ijkl}^{e} \dot{\varepsilon}_{kl} \tag{34}$$

here

$$\psi = \frac{\partial f}{\partial \sigma_{ij}} D_{ijkl}^{e} \frac{\partial f}{\partial \sigma_{kl}} + \left(H' - \frac{\partial f}{\partial \bar{\varepsilon}^{p}} \right) \sqrt{\frac{2}{3} \frac{\partial f}{\partial \sigma_{ij}} \frac{\partial f}{\partial \sigma_{ij}}} - \frac{\partial f}{\partial \varepsilon_{ij}^{p}} \frac{\partial f}{\partial \sigma_{ij}} \tag{35}$$

where $H' = \partial k / \partial \bar{\varepsilon}^{p}$ is the local slope of the uniaxial stress/plastic strain curve, which can be determined experimentally.

It is noted that Eqs. (34) and (35) are similar to those used by Banerjee et al. (1989) and from Eq. (4) we can see that Eq. (33) can be reduced to the Drucker normality rule (e.g., Owen and Hinton, 1980).

4.2. System equations formulated in terms of the plastic multiplier

The elastic stress increments can be defined as (e.g., Telles, 1983):

$$\dot{\sigma}_{ij}^{e} = D_{ijkl}^{e} \dot{\varepsilon}_{kl} \tag{36}$$

The total number of nodes is denoted by N. For each node, say node n, from Eq. (5) we have (in matrix form):

$$\{\dot{\sigma}^{e}\}_{(n)} = \{\dot{\sigma}\}_{(n)} + \{\dot{\sigma}^{p}\}_{(n)} \tag{37}$$

Eqs. (33) and (34) can be written in matrix forms as:

$$\{\dot{\sigma}^{p}\}_{(n)} = \left\{d^{f}\right\}_{(n)} \dot{\lambda}_{(n)} \tag{38}$$

$$\dot{\lambda}_{(n)} = \left\{\nabla f_{\psi}\right\}_{(n)}^{t} \{\dot{\sigma}^{e}\}_{(n)} \tag{39}$$

where

$$\left\{d^{f}\right\}_{(n)} = [D^{e}] \left\{ \frac{\partial f}{\partial \sigma} \right\}_{(n)} \tag{40}$$

$$\left\{\nabla f_{\psi}\right\}_{(n)} = \frac{1}{\psi} \left\{ \frac{\partial f}{\partial \sigma} \right\}_{(n)} \tag{41}$$

A global initial stress vector can be formed from Eq. (38) as:

$$\{\dot{\sigma}^p\} = [d^f]\{\dot{\lambda}\} \tag{42}$$

where $[d^f]$ is a $6N \times N$ diagonally dominant sparse matrix, formed by Eq. (40).

Inverting Eq. (29) and using Eq. (42), it follows that:

$$\{\dot{X}\} = \{\dot{Y}^e\} + [A^e][d^f]\{\dot{\lambda}\} \tag{43}$$

where

$$\{\dot{Y}^e\} = [A^b]^{-1}\{\dot{Y}^b\} \tag{44}$$

$$[A^e] = [A^b]^{-1}[E^b] \tag{45}$$

Substituting Eqs. (42) and (43) into (30), leads to:

$$\{\dot{\sigma}\} = \{\dot{Y}^e\} + [E][d^f]\{\dot{\lambda}\} \tag{46}$$

where

$$\{\dot{Y}^e\} = \{\dot{Y}^\sigma\} + [A^\sigma]\{\dot{Y}^e\} \tag{47}$$

$$[E] = [E^\sigma] + [A^\sigma][A^e] \tag{48}$$

Substituting Eqs. (46) and (42) into the global form of Eq. (37), and the result into (39), we obtain:

$$\{\dot{\lambda}\} = [\nabla f_\psi]\Big(\{\dot{Y}^e\} + [E][d^f]\{\dot{\lambda}\} + [d^f]\{\dot{\lambda}\}\Big) \tag{49}$$

where $[\nabla f_\psi]$ is a $N \times 6N$ diagonally dominant matrix, formed by$\{\nabla f_\psi\}^t_{(n)}$ (see Eq. (41)). Rearranging (49), we obtain the system equations as:

$$[A^\lambda]\{\dot{\lambda}\} = \{\dot{Y}^f\} \tag{50}$$

where

$$[A^\lambda] = [I] - [\nabla f_\psi][C][d^f] \tag{51}$$

$$\{\dot{Y}^f\} = [\nabla f_\psi]\{\dot{Y}^e\} \tag{52}$$

In which, $[C]$ is a constant matrix:

$$[C] = [I] + [E] \tag{53}$$

Once the plastic multipliers $\{\dot{\lambda}\}$ are obtained from Eq. (50), the increments of the boundary unknowns and stresses can be computed using Eqs. (43) and (46), respectively. Only $[\nabla f_\psi]$ and $[d^f]$ (obtained from Eqs. (41) and (40), respectively) are functions of stress. Thus, the Newton–Raphson iterative process can be easily applied to solve these system equations.

4.3. Newton–Raphson iterative algorithm

The notation $\{\sigma\}_n$, $\{X\}_n$ and $\{\lambda\}_n$ is used to denote the stress, boundary unknown and plastic multiplier vectors, respectively, at the end of the nth increment. For the new increment, we use $\{\sigma\}^i$, $\{X\}^i$ and $\{\lambda\}^i$ to denote the results after the ith iteration. The residual of Eq. (50) can be written as:

$$\{R\}^i = \left\{\dot{Y}^f\right\}^i - \left[A^\lambda\right]^i\left(\{\lambda\}^i - \{\lambda_n\}\right) \tag{54}$$

To reduce the residual to a specified tolerance, forcing $\{R\}^{i+1}$ to be zero produces:

$$0 = \{R\}^{i+1} = \{R\}^i + \frac{\partial\{R\}^i}{\partial\{\lambda\}^i}\{\Delta\dot{\lambda}\} = \{R\}^i - \left[A^\lambda\right]^i\{\Delta\dot{\lambda}\} \tag{55}$$

where $\{\Delta\dot{\lambda}\}$ are the changes in the plastic multiplier. From Eq. (55), we obtain:

$$\left[A^\lambda\right]^i\{\Delta\dot{\lambda}\} = \{R\}^i \tag{56}$$

Solving Eq. (56) for $\{\Delta\dot{\lambda}\}$, we can obtain the changes in plastic multiplier. Then, the corresponding changes in boundary unknowns and stresses can be computed by:

$$\{\Delta\dot{X}\} = [A^c]\left[d^f\right]^i\{\Delta\dot{\lambda}\} \tag{57}$$

$$\{\Delta\dot{\sigma}\} = [E]\left[d^f\right]^i\{\Delta\dot{\lambda}\} \tag{58}$$

The values of the variables need to be updated by:

$$\{\lambda\}^{i+1} = \{\lambda\}^i + \{\Delta\dot{\lambda}\} \tag{59}$$

$$\{X\}^{i+1} = \{X\}^i + \{\Delta\dot{X}\} \tag{60}$$

$$\{\sigma\}^{i+1} = \{\sigma\}^i + \{\Delta\dot{\sigma}\} \tag{61}$$

This iterative process can be described as follows:

1. Impose load increment $\{\dot{Y}^c\}$ and $\{\dot{Y}^e\}$ using Eqs. (44) and (47).
2. Scale stresses for each node:

$$\{\sigma^t\} = \{\sigma\}_n + \{\dot{Y}^e\}$$

IF $F(\sigma^t) \le 0$ THEN $\{\sigma\}_n = \{\sigma^t\}$
ELSE IF $F(\sigma_n) < 0$ THEN

$$\alpha = \frac{-F(\sigma_n)}{F(\sigma^t) - F(\sigma_n)}; \quad \{\sigma\}_n = \{\sigma\}_n + \alpha\{\dot{Y}^e\}; \quad \{\dot{Y}^e\} = (1-\alpha)\{\dot{Y}^e\}$$

3. Initialise iterative variables for each node:

$$i=0;\quad \{\sigma\}^i=\{\sigma\}_n+\{\dot{Y}^e\};\quad \{X\}^i=\{X\}_n+\{\dot{Y}^c\};\quad \{\lambda\}^i=\{\lambda\}_n$$

4. Evaluate $[A^\lambda]^i$ and $\{\dot{Y}^f\}^i$ using Eqs. (51) and (52) in terms of stress state $\{\sigma\}^i$.
5. Calculate residual $\{R\}^i$ using Eq. (54).
6. Check convergence:
   IF $|\{R\}^i|$ < TOLER THEN GOTO 1 for next increment

7. Solve system equations for $\{\Delta\dot{\lambda}\}$ using Eq. (56)
8. Evaluate changes in boundary unknowns and stresses using Eqs. (57) and (58).
9. Evaluate changes in internal variables:

$$\{\Delta\dot{\varepsilon}^p\}=[\partial f/\partial\sigma]\{\Delta\dot{\lambda}\};\quad \{\Delta\dot{\bar{\varepsilon}}^p\}=\sqrt{2/3\{\Delta\dot{\varepsilon}^p\}^t\{\Delta\dot{\varepsilon}^p\}}$$

10. Update variables for each node using Eqs. (59)–(61) and $k(\bar{\varepsilon}^p)=k(\bar{\varepsilon}^p)+H'\Delta\dot{\bar{\varepsilon}}^p$
11. $i=i+1$; GOTO 4 for next iteration.

It is of importance to note that in the above process, the matrices $[\nabla f_\psi]$ and $[d^f]$ are zero for elastic nodes. Therefore, the number of degrees of freedom of the system (Eq. (50)) is equal to the number of yield nodes in the current increment. This feature can save substantial computational time. Further, $[C]$, $[A^c]$ and $[E]$ in Eqs. (51), (57) and (58), respectively, are constant matrices. Once they are formed and stored, they can be used directly. Also, the matrices $[\nabla f_\psi]$ and $[d^f]$ need not be formed in computation, because they can be directly incorporated into the matrices $[A^\lambda]$ and $\{\dot{Y}^f\}$ during the assembly process. Although inversion of matrix $[A^b]$ is needed (in Eqs. (44) and (45)), the computational cost is small since its dimension is related to the number of boundary nodes alone and the inversion is carried out once only. This process has therefore distinct advantages over existing Newton–Raphson iterative techniques (Chopra and Dargush, 1994) which operate on the entire system equations (boundary + internal).

5. Numerical examples

The boundary element solution of elastoplasticity is evidently complex and should be thoroughly validated. This section describes some work carried out for this purpose using the computer code (***NLBEAS***) which was developed using the method described in this paper. The detailed description of

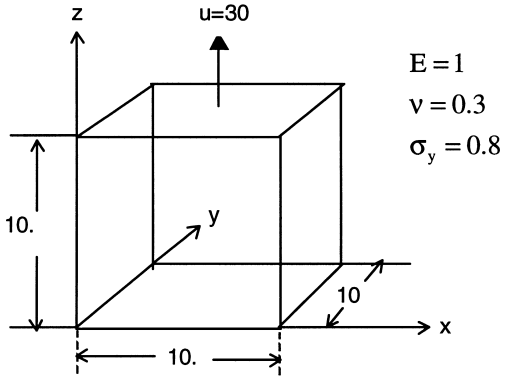

Fig. 6. A cube under tension.

Table 1
Results for the cube centre ($H' = 0.1$)

	σ_{zz}	ε_{zz}^{p}	u_z	u_x
Linear cell and element	1.0000	2.0000	15.000	−6.500
Quadratic cell and element	0.9999	1.997	14.992	−6.498
Analytical	1.0	2.0	15.0	−6.5

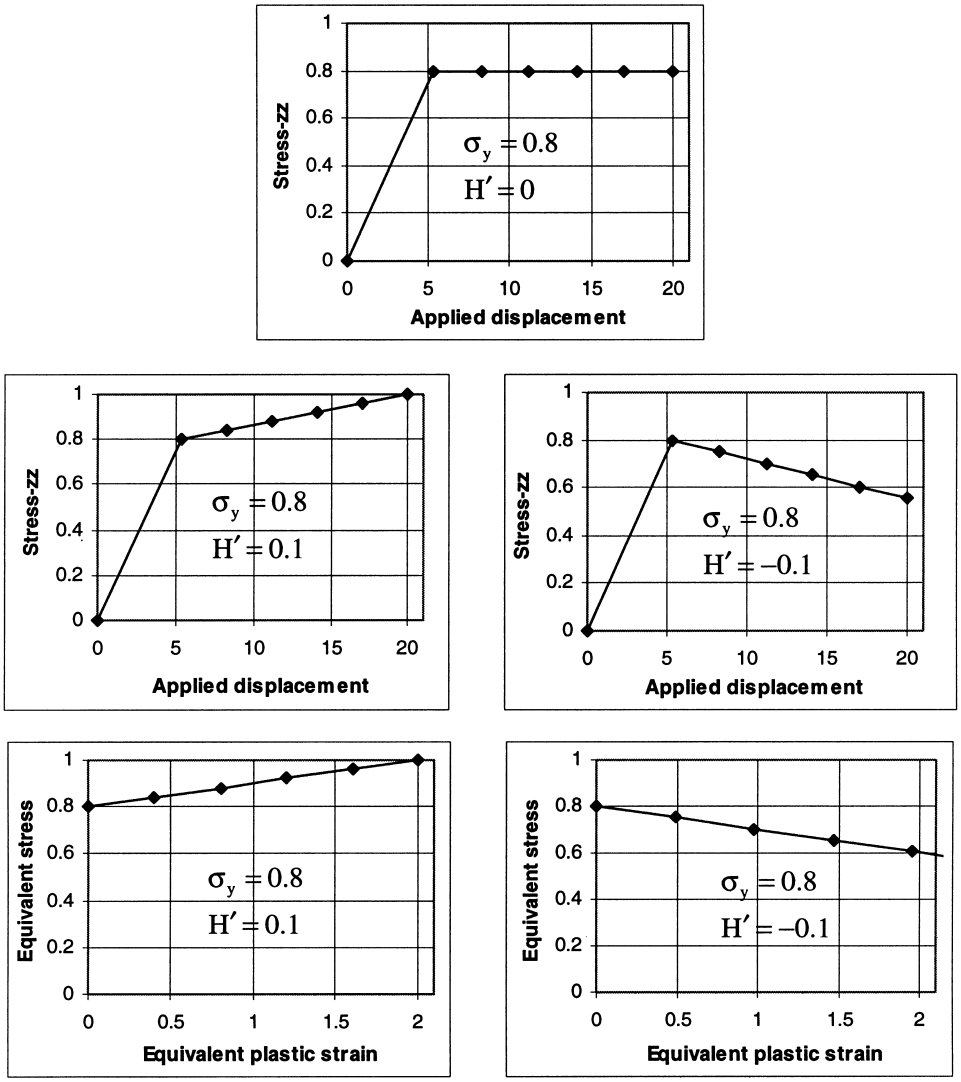

Fig. 7. Hardening, perfect plasticity, and softening performance.

Table 2
Convergence of iterative process

Increment	No. of degees of freedom	Iterations	Value of $\|\{R\}^i\|/\sigma_y$ for every iteration
1	13	3	8.513E−2, 1.502E−3, 2.801E−5
5	20	3	1.116E−1, 2.258E−3, 5.774E−5
10	40	4	1.369E−1, 3.188E−3, 1.196E−4, 5.374E−6
15	80	5	1.512E−1, 6.432E−3, 1.047E−3, 1.640E−4, 2.365E−5

this program and more complicated examples can be found in Gao (1999). Only three examples are given in the following, which were computed using single precision arithmetic on a Pentium PC (233 MHz, 64 Mb RAM). Computational times on the current generation of micro-computers may be of the order of magnitude less than those quoted here.

5.1. 3D Cube under uniaxial tension

This first example deals with a cube subjected to tensile displacement (Fig. 6). The material satisfies the *Von Mises criterion*, and this example is intended to illustrate hardening, perfect plasticity, and softening phenomena under uniaxial loading.

The cube was discretized by four boundary elements per surface and eight volume cells and the 'roller' condition was imposed on the three planes $x = 0$, $y = 0$ and $z = 0$. The computation is displacement-controlled. Table 1 gives the computed results at the cube centre for a linear hardening case ($H' = 0.1$), using linear and quadratic elements and cells. From Table 1 it is observed that the results calculated by the current method are in excellent agreement with the analytical solution.

Fig. 7 shows computed results for the perfect plasticity ($H' = 0$), hardening ($H' = 0.1$), and softening ($H' = -0.1$). All of these results are, essentially, exact and illustrate the capacity of the program to cope with the spectrum of hardening rules.

In this problem, the results are essentially independent of increment size and in each increment convergence can be achieved only using one iteration, provided that stress-scaling is carried out when the trial stresses $\{\sigma^t\}$ cross the yield surface. The total computational time is 140 s for the quadratic elements and cells with 81 nodes (including 74 boundary nodes), 24 boundary elements and 8 cells.

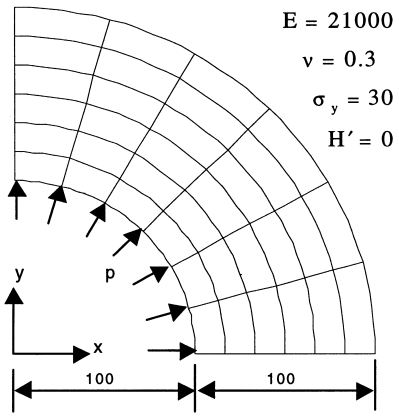

Fig. 8. Mesh and material properties of an internally pressurised thick cylinder.

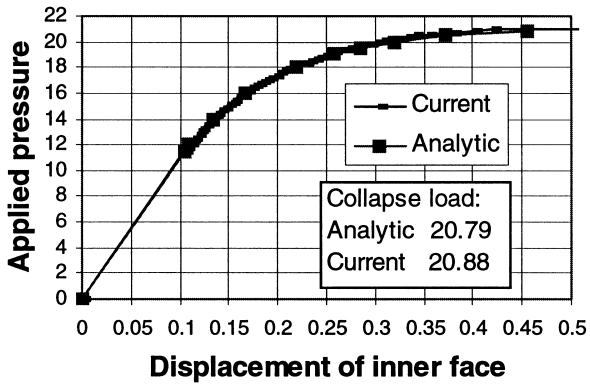

Fig. 9. Displacement of the inner surface with increasing pressure.

5.2. 2D thick-wall cylinder under internal pressure

The second numerical example considered is a thick cylinder subjected to internal pressures (Fig. 8), under plane strain conditions. Due to symmetry, a quarter of the cylinder is analysed using quadratic boundary elements and cells. The discretization consists of 133 nodes (including 26 boundary nodes), 12 boundary elements and 36 cells. The *Tresca* yield criterion is assumed and the numerical solutions obtained are compared with the theoretical results of Lubliner (1990). The pressure/radial displacement characteristics are shown in Fig. 9 and radial and circumferential (hoop) stress distributions for a specified pressure value, $p = 18$, are plotted in Fig. 10.

To examine the dependence of the results on load increment size, plots of radial and hoop stress against the number of the increments (for radius $r = 100$ (inner surface) and $r = 150$ (middle surface)), are produced in Fig. 11 for the case of $p = 20$.

Fig. 11 shows that, at the inner surface, a stable solution is obtained using very few increments of loading. However, at least 15 load increments have to be used for the case of the pressure $p = 20$ to capture a stable internal solution. Table 2 gives some data on the convergence of the iterative process for the case of $p = 20$, where the total number of the increments is 15 and the total computational time is 85 s. The rapid convergence of the algorithm is evident (tolerance = 1.0E−4).

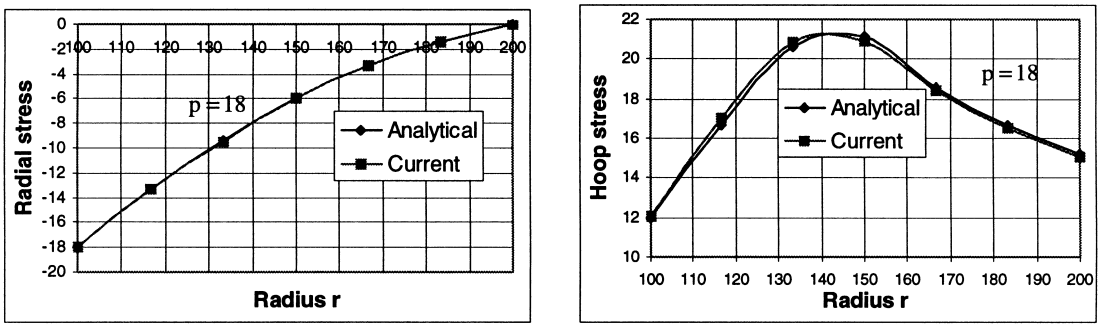

Fig. 10. Radial and hoop stresses along radius.

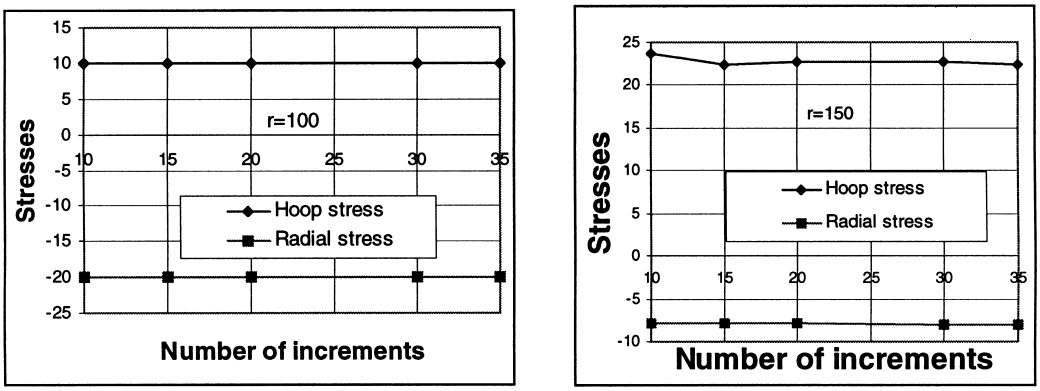

Fig. 11. Stresses versus number of increments ($p = 20$).

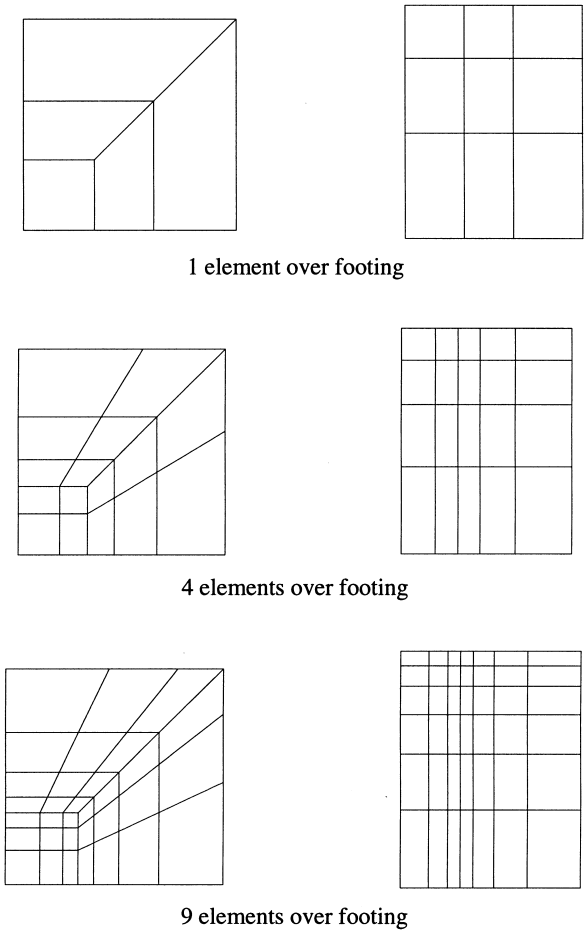

Fig. 12. Boundary elements and internal cells for footing problem.

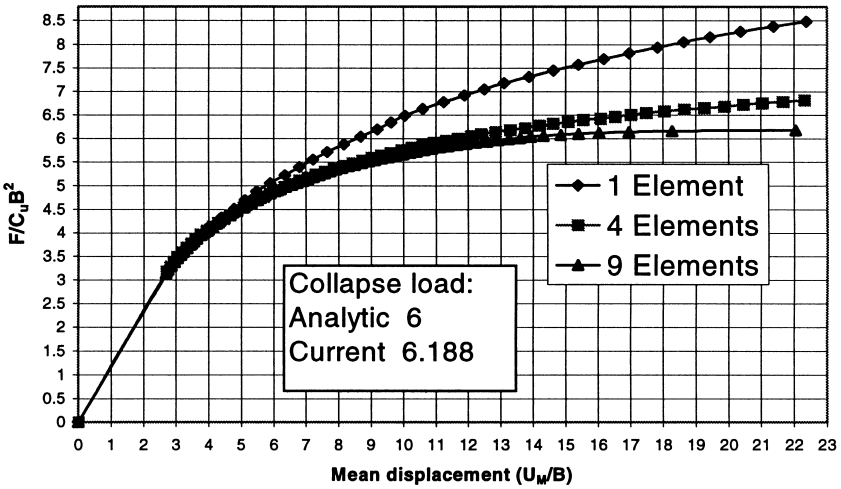

Fig. 13. Load versus mean settlement, for a square flexible footing.

5.3. 3D flexible footing

This example pertains to the collapse behaviour of a square footing (with dimension $B = 1$) on the surface of a half-space. It is conventional practice to express the collapse load in terms of the undrained shear strength (C_u) of the soil. From the definition of the equivalent stress σ_y (uniaxial tension yield limit) which characterises the von Mises yield criterion, it can be easily shown that $\sigma_y = 2C_u$. The computation was carried out using quadratic boundary elements and internal cells. The far-field ground surface was discretized using progressively larger boundary elements (Gao and Davies, 1998). At each node shared by the footing and ground surface, two nodes were used to model the traction-discontinuity (Gao, 1999). Young's modulus $E = 1000$ and Poison's ratio $\nu = 0.3$ are assumed through out. The displacements in the following figures should be divided by 10^3 to recover the actual displacements. A uniform vertical pressure is applied on the footing and quadrantal symmetry is utilised. To examine the convergence characteristics, three analyses were performed: (a) 155 nodes (including 48 boundary nodes), 11 boundary elements and 15 cells; (b) 476 nodes (including 119 boundary nodes), 32 boundary elements and 64 cells; and (c) 1197 nodes (including 200 boundary nodes), 57 boundary elements and 198 cells. The number of elements over (the quadrant of) the footing is one, four and nine, respectively.

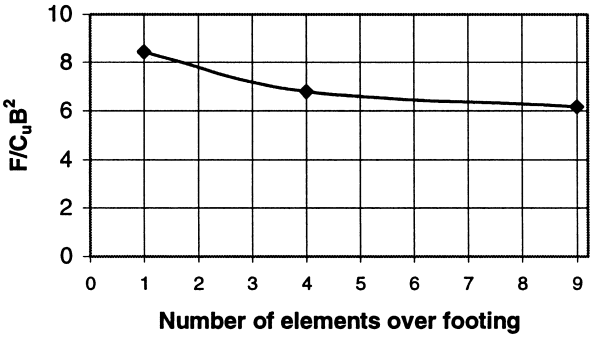

Fig. 14. Convergence of footing collapse load solutions.

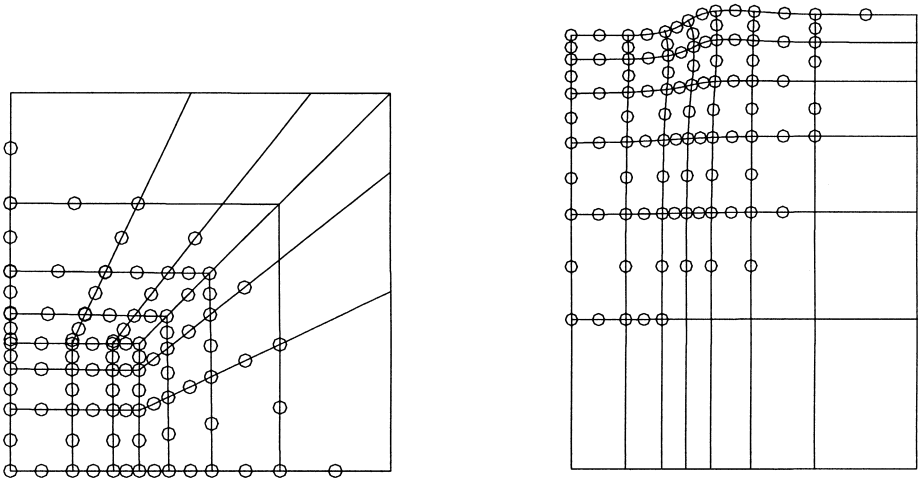

Fig. 15. Deformed mesh and yield nodes for 9 element case (near collapse).

Fig. 12 shows the meshes for each case (over the expected yield region only), depicting both the boundary elements and the corresponding cells in plan and in transverse section. Fig. 13 is load-placement plots, where the 'mean' displacement is approximated using the equation (Fox, 1948) $u_M = (u_{\text{corner}} + 2u_{\text{centre}})_{\text{flexible}}/3$. This should yield approximately the same displacement as a rigid footing.

Fig. 13 shows that there is little difference between the results up to a load level of $4.5C_uB^2$. The coarse discretizations however fail to capture the collapse (at about $6C_uB^2$) and instead return a monotonically increasing function to higher load levels. The convergence characteristics are more clearly illustrated in Fig. 14. The relatively small difference between the results for four elements (over the footing quadrant) with respect to results for nine elements suggests that convergence is very nearly achieved at the latter level.

Fig. 15 identifies which nodes yield (near to collapse) in plan and in transverse section. The yield region extends laterally to encompass an area equal to at least four times the footing area and to a depth rather greater than the footing width.

The exact solution to this problem is not known. However, the collapse load for a rigid circular footing under the same condition is given by $F_e = 6A_cC_u$ (Banerjee and Davies, 1984) where A_c is the area of the footing, and it is probable that the collapse load for a square footing will not be much greater. Forty increments are used for this example and convergence is also excellent. The maximum number of iterations was six and computational time for 1197 nodes was 14 h.

6. Conclusions

In this paper, an effective boundary element algorithm for 2D and 3D elastoplastic problems is developed. Semi-analytical methods are developed to integrate the strongly singular domain integrals. The numerical integrations are performed only over the cell boundaries surrounding the source point, leading to substantial savings in computational time.

The system equations are formulated in terms of the plastic multipliers (only), with the result that the number of degrees of freedom is equal to the number of the current yield nodes. This novel feature allows the solution of larger problems than would otherwise be possible. Several numerical examples demonstrate that the proposed Newton–Raphson iterative solution scheme exhibits excellent convergence.

References

Banerjee, P.K., Cathie, D.N., Davies, T.G., 1979. Two and three-dimensional problems of elasto-plasticity. In: Developments in Boundary Element Methods. Elsevier, London.

Banerjee, P.K., Davies, T.G., 1979. Analysis of some case histories of laterally loaded pile groups. In: Proc. of Int. Conf. On Numerical Methods in Offshore Piling. Institution of Civil Engineers, London.

Banerjee, P.K., Davies, T.G., 1984. Advanced implementation of the boundary element methods for three-dimensional problems of elasto-plasticity. In: Developments in Boundary Element Methods. Elsevier, London.

Banerjee, P.K., Raveendra, S.T., 1986. Advanced boundary element analysis of two- and three-dimensional problems of elasto-plasticity. Int. J. Num. Meth. Engng 23, 985–1002.

Banerjee, P.K., Henry, D.P., Raveendra, S.T., 1989. Advanced inelastic analysis of solids by the boundary element method. Int. J. Mech. Sci 31, 309–322.

Banerjee, P.K., 1994. The Boundary Element Methods in Engineering. McGraw-Hill, New York, pp. 73–75.

Bonnet, M., Mukherjee, S., 1996. Implicit BEM formulations for usual and sensitivity problems in elasto-plasticity using the consistent tangent operator concept. Int. J. Solids Structures 33, 4461–4480.

Brebbia, C.A., Telles, J.C.F., Wrobel, L.C., 1984. Boundary Element Techniques. Springer, Berlin, New York.

Bui, H.D., 1978. Some remarks about the formulation of three-dimensional thermoelastoplastic problems by integral equations. Int. J. Solids and Structures 14, 935–939.

Burghardt, B., Van, A.L., 1998. A fully regularized direct boundary formulation for three-dimensional elastoplastic problems. In: Kassab, A., Brebbia, C.A., Chopra, M. (Eds.), Boundary Element XX, Computational Mechanics Publications, Southampton, U.K.

Chandra, A., Saigal, S., 1991. A boundary element analysis of the axisymmetric extrusion process. In. J. Nonlinear Mech 26, 1–13.

Chandra, A., Mukherjee, S., 1996. Boundary Element Methods in Manufacturing. Oxford University Press, Oxford, UK.

Chen, W.F., Han, D.J., 1988. Plasticity for Structural Engineers. Springer-Verlag, London.

Chen, Z.Q., Ji, X., 1987. Boundary element analysis of finite deformation problems of elasto-plasticity. In: Tanaka, M., Du, Q. (Eds.), Theory and Application of Boundary Element Methods, Proc. First Japan–China Symp. On Boundary Element Methods. Pergamon, Oxford, pp. 261–270.

Chen, H., Wang, Y.C., Lu, P., 1996. Stress rate integral equations of elastoplasticity. ACTA Mechanica Sinica (English Series) 12, 55–64.

Chopra, M.B., Dargush, G.F., 1994. Development of BEM for thermoplasticity. Int. J. Solids Structures 31, 1635–1656.

Cisilino, A.P., Aliabadi, M.H., Otegui, J.L., 1998. A three-dimensional boundary element formulation for the elastoplastic analysis for cracked bodies. Int. J. Numer. Meth. Engng 42, 237–256.

Crisfield, M.A., 1997. Non-linear Finite Element Analysis of Solids and Structures. Wiley, Chichester, UK.

Dallner, R., Kuhn, G., 1993. Efficient evaluation of volume integrals in boundary element method. Comp. Methods in Appl. Mech. and Engng 109, 95–109.

Dong, C.Y., Antes, H., 1998. An improved inner point stress integral equation and its application in 2-D elastoplastic problems. Engineering Analysis with Boundary Elements 22, 133–139.

Fox, E.N., 1948. The mean elastic settlement of a uniformly loaded area at a depth below the ground surface. Proc. 2nd Int. Conf. Soil Mechs. Fndn. Eng 1, 129.

Gao, X.W., Davies, T.G., 1999a. 3D multi-region BEM with corners and edges. International Journal of Solids and Structures, in press.

Gao, X.W., Davies, T.G., 1999b. Adaptive algorithm in elasto-plastic boundary element analysis. Journal of the Chinese Institute of Engineers, submitted.

Gao, X.W., Davies, T.G., 1998. 3-D infinite boundary elements for half-space problems. Engineering Analysis with Boundary Elements 21, 207–213.

Gao, X.W., 1999. 3D non-linear and multi-region boundary element stress analysis. PhD Thesis, University of Glasgow, UK.

Gao, X.W., Zhong, Z.Q., 1992. Elastoplastic damage theory in isotropic medium. Chinese Journal of Theoretical and Applied Mechanics 4.

Gao, X.W., Lu, J.T., 1992. A combination method of FEM and BEM for elastoplastic problems. In: Proc. of Forth Int. Conf. on EPMESC, Dalian, China, August.

Gao, X.W., Zheng, Y.R., 1990. An accelerating convergence method for elastoplastic iterative computation in strain space. In: Proc. of Third Int. Conf. on EPMESC, MACAU, 84–90.

Guiggiani, M., Gigante, A., 1990. A general algorithm for multidimensional Cauchy principal value integrals in the boundary element method. J. Appl. Mech 57, 906–915.

Guiggiani, M., Krishnasamy, G., Rudolphi, T.J., Rizzo, F.J., 1992. General algorithm for the numerical solution of hyper-singular boundary integral equations. ASME J. Appl. Mech 59, 604–614.

Henry, D.P., 1987. Advanced development of the boundary element method for elastic and inelastic thermal stress analysis. PhD Dissertation, State University of New York at Buffalo.

Henry, D.P., Banerjee, P.K., 1988. A variable stiffness type boundary element formulation for axisymmetric elastoplastic media. Int. J. Num. Meth. Engng 26, 1005–1027.

Huber, O., Dallner, R., Partheymuller, P., Kuhn, G., 1996. Evaluation of the stress tensor in 3-D elastoplasticity direct solving of hypersingular integrals. Int. J. Num. Meth. Engng 39, 2555–2573.

Huang, Q., Du, Q., 1988. An improved formulation for domain stress evaluation by boundary element methods in elastoplastic problems. In: Proc. China–US Seminar on Boundary Integral Equations and Finite Element Methods in Physics and Engineering, Xian, China.

Il'iushin, A.A., 1961. On the postulate of plasticity. Prikl. Mat. Meh 25, 503–507.

Kane, J.H., 1994. Boundary Element Analysis in Engineering Continuum Mechanics. Prentice-Hall, Englewood Cliffs, NJ.

Krishnasamy, G., Rizzo, F.J., Rudolphi, T.J., 1992. Hypersingular boundary integral equations: Their occurrence, interpretation, regularization and computation. In: Banerjee, P.K., Kobayashi, S. (Eds.), Advanced Dynamic Analysis by Boundary Element Methods. Elsevier, London and New York, pp. 207–252.

Kumar, V., Mukherjee, S., 1977. A boundary-integral equation formulation for time-dependent inelastic deformation in metals. Int. J. Mechanical Science 19, 713–724.

Lachat, J.C., 1975, A further development of the boundary integral technique for elastostatics. PhD Thesis, University of Southampton.

Lee, K.H., Fenner, R.T., 1986. A quadratic formulation for two-dimensional elastoplastic analysis using the boundary integral equation method. J. Strain Analysis 21 (3), 159–175.

Lubliner, J., 1990. Plasticity Theory. Macmillan, New York, London.

Mendelson, A., Albers, L.V., 1975. An application of the boundary integral equation method to elastoplastic problems. In: Cruse, T.A., Rizzo, F.J. (Eds.), Proc. ASME Conf. on boundary integral equation methods, AMD 11, New York.

Mukherjee, S., 1977. Corrected boundary integral equations in planar thermo-elastoplasticity. Int. J. Solids Structures 13, 331–335.

Mukherjee, S., 1982. Boundary Element Method in Creep and Fracture. Applied Science Publishers, New York.

Mustoe, G.G.W., 1984. Advanced integration schemes over boundary elements and volume cells for two- and three-dimensional non-linear analysis. In: Developments in Boundary Element Methods. Elsevier, London.

Naghdi, P.M., Trapp, J.A., 1975. The significance of formulating plasticity theory with reference to loading surfaces in strain space. Int. J. Eng. Sci 13, 785–797.

Owen, D.R.J., Hinton, E., 1980. Finite Elements in Plasticity: Theory and Practice. Pineridge, Swansea, UK.

Poon, H., Mukherjee, S., Ahmad, M.F., 1998a. Use of 'simple solutions' in regularizing hypersingular boundary integral equations in elastoplasticity. ASME J. Appl. Mech 65, 39–45.

Poon, H., Mukherjee, S., Bonnet, M., 1998b. Numerical implementation of a CTO-based implicit approach for the BEM solution of usual and sensitivity problems in elasto-plasticity. Engineering Analysis with Boundary Elements 22, 257–269.

Raveendra, S.T., 1984. Advanced development of BEM for two and three-dimensional inelastic analysis. PhD Dissertation, State University of New York at Buffalo.

Riccardella, P., 1973. An implementation of the boundary integral technique for planar problems of elasticity and elastoplasticity. PhD Thesis, Carnegie-Mellon University, Pittsurgh, PA.

Simo, J.C., Taylor, R.L., 1985. Consistent tangent operators for rate-independent elastoplasticity. Comp. Meth. Appl. Mech. Engng 48, 101–118.

Swedlow, J.L., Cruse, T.A., 1971. Formulation of boundary integral equations for three-dimensional elasto-plastic flow. Int. J. Solids and Structures 7, 1673–1683.

Telles, J.C.F., 1983. The Boundary Element Method Applied to Inelastic Problems. Springer-Verlag, Berlin.

Telles, J.C.F., Brebbia, C.A., 1979. On the application of the boundary element method to plasticity. Appl. Math. Modelling 3, 466–470.

Telles, J.C.F., Brebbia, C.A., 1980. The boundary element method in plasticity. In: Proc. Second Int. Conf. on Recent Advances in Boundary Element Methods. Pentech Press, Plymouth, 295–317.

Telles, J.C.F., Carrer, J.A.M., 1991. Implicit procedures for the solution of elastoplastic problems by the boundary element method. Math. Comput. Modelling 15, 303–311.

Wearing, J.L., Dimagiba, R.R.M., 1998. The development of the boundary element method for three dimensional elasto-plastic analysis. In: Brebbia (Ed.), Boundary Element Research in Europe, Computational Mechanics Publications, pp. 93–102, Southampton, U.K.

Zhang, Q., Mukherjee, S., Chandra, A., 1992. Design sensitivity coefficients for elastoviscoplastic problems by boundary element methods. Int. J. Num. Meth. Engng 34, 947–966.

Zheng, Y.R., Gao, X.W., 1986. Application of elastoplastic BEM to back analysis. Journal of Underground Technology 2.

Zheng, Y.R., Xu, G.C., Gao, X.W., 1989. The coupled computational method of elastoplastic BEM and FEM. Chinese Journal of Engineering Mechanics 1.